Telecom-band degenerate-frequency photon pair generation in silicon microring cavities

Yuan Guo, Wei Zhang,* Shuai Dong, Yidong Huang, and Jiangde Peng

Tsinghua National Laboratory for Information Science and Technology, Department of Electronic Engineering, Tsinghua University, Beijing 100084, China

**Corresponding author: zwei@Tsinghua.edu.cn*

Received January 10, 2014; revised March 17, 2014; accepted March 18, 2014; posted March 18, 2014 (Doc. ID 204492); published April 15, 2014

In this Letter, telecom-band degenerate-frequency photon pairs are generated in a specific mode of a silicon microring cavity by the nondegenerate spontaneous four-wave mixing (SFWM) process, under two continuous-wave pumps at resonance wavelength of two different cavity modes. The ratio of coincidence to accidental coincidence is up to 100 under a time bin width of 5 ns, showing their characteristics of quantum correlation. Their quantum interference in balanced and unbalanced Mach–Zehnder interferometers is investigated theoretically and experimentally, and the results show potential in quantum metrology and quantum information.

OCIS codes: (270.0270) Quantum optics; (190.4390) Nonlinear optics, integrated optics; (190.4380) Nonlinear optics, four-wave mixing.

http://dx.doi.org/10.1364/OL.39.002526

Silicon microring cavities are promising candidates for correlated photon pair generation at the telecom band. The silicon waveguide has an ultrahigh nonlinear coefficient thanks to the high $\chi^{(3)}$ of silicon and the high light confinement of the waveguide [1], while the nonlinearity in the cavity would be further improved by the light field enhancement if the input light was on resonance [2–4]. Hence, correlated photon pairs can be generated under ultralow pump powers in silicon microring cavities [5–7]. On the other hand, since in silicon waveguides, noise photons generated by the spontaneous Raman scattering are restricted to a narrow band and are easily filtered out, low noise performance could be realized by silicon waveguides even at room temperature [8]. Although free carrier absorption in the silicon microring cavity would cause performance degradation, recent works have shown that it can be overcome by the reverse-biased p-i-n structure in silicon waveguides [9]. Hence, the microring cavity is an attractive platform for integrated quantum light sources. Up to now, all the experiments on photon pair generation in silicon microring cavities have been based on degenerate spontaneous four-wave mixing (SFWM) [10], in which the generated photon pairs are nondegenerate, i.e., the signal and idler photons are in two different cavity modes under a monochromatic pump light.

As an important resource, degenerate-frequency photon pairs have many applications such as quantum state engineering [11] and quantum metrology [12]. To realize the degenerate-frequency photon pair generation, the nondegenerate SFWM process should be used, which needs two pump lights with different wavelengths. It has been demonstrated in optical fibers [13,14] and silicon waveguides [15], but has not been realized in silicon microring cavities.

In this Letter, degenerate-frequency photon pairs at the telecom band are generated in a specific mode of a silicon microring cavity by the nondegenerate SFWM process. The photo of the silicon microring cavity sample used in the experiment is shown in Fig. 1(a), which is fabricated by standard CMOS processes [Institute of Microelectronics (IME), Singapore]. The cavity has the shape of a race track, with a circumference of 132.5 μm. It is coupled with a bus waveguide 3 mm in length. All the waveguides in the sample have a deep ridge structure, with a width of 450 nm, total height of 220 nm, and ridge height of 160 nm. Light is coupled into and out of the bus waveguide as the quasi-TE mode through two lensed fibers. Inverted taper structures are fabricated at both ends of the bus waveguide to reduce the coupling loss. Figure 1(b) shows the transmission spectrum measured by a swept test system, including a tunable laser (Santec TSL-510, with a wavelength resolution of 1 pm) and a detector (Agilent 81636B). It can be seen that the insertion loss of the bus waveguide is 5.6 dB, mainly due to the coupling loss. Dips in the spectrum indicate cavity modes. In the experiment, the modes at 1533.80 and 1551.52 nm are for the two pumps, and the photon pairs are generated in the mode at 1542.60 nm. Characteristics of the three modes are

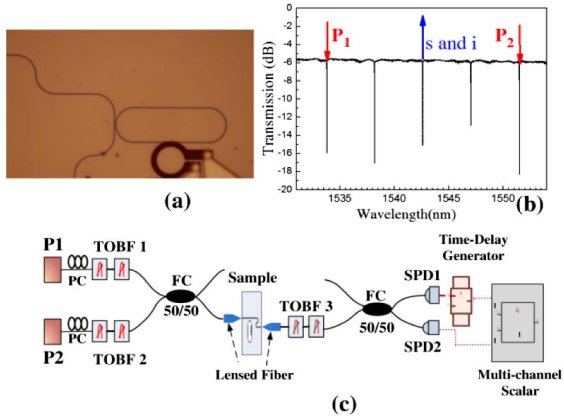

Fig. 1. Experiment setup. (a) Photo of the silicon microring cavity sample. (b) Transmission spectrum of the sample, showing the three cavity modes used in the experiment. (c) Sketch of the experiment setup. PC, polarization controller; TOBF, tunable optical bandpass filter; FC, 50/50 fiber coupler; SPD, single-photon detector.

Table 1. Characteristics of the Cavity Modes

Resonance Wavelength (nm)	Resonance FWHM (nm)	Extinction Ratio (dB)	Q Factor
1533.80	0.019	10.3	8.1×10^4
1551.52	0.024	12	6.5×10^4
1542.60	0.023	9	6.8×10^4

shown in Table 1. The extinction ratios of the three modes are all higher than 9 dB, showing that they are close to critical coupling. Q values of the three modes are all at the magnitude of 10^4–10^5, hence, it can be expected that photon pairs could be generated under quite low pump levels due to the field enhancement of the cavity.

The experiment setup is shown in Fig. 1(c). Two tunable lasers provide the two pumps (denoted by P1 and P2). Their wavelengths are tuned to two cavity modes, as shown in Fig. 1(b). Each of them has a narrow linewidth of 100 kHz. Their polarizations are adjusted by two fiber polarization controllers. Their sideband suppressions at the resonance wavelength for the photon pair generation are improved to 130 dB through two tunable optical bandpass filter systems (TOBF1 and TOBF2). The two pumps are combined by a 50/50 fiber coupler (50/50 FC), and then coupled into the bus waveguide by a lensed fiber. Through the nondegenerate SFWM process in the cavity, photon pairs are generated in the central cavity mode shown in Fig. 1(b). At the output end, another filter system (TOBF3, with an insertion loss of 4 dB) is utilized to select the photon pairs. Then generated photons are directed to two single-photon detectors (SPD1 and SPD2, id220, IDQ) by another 50/50 FC. The efficiencies and dead times of the two SPDs are 10% and 10 μs, respectively. Hence, the total photon collection and detection efficiency in this experiment setup is about 19 dB, including the coupling loss of the bus waveguide, the insertion loss of TOBF3, the 50/50 FC at the output end, and the detection efficiencies of the two SPDs. The output of SPD2 is connected to the trigger port of a multichannel scalar (SR430, SRS), while the output of SPD1 is connected to the signal port of the multichannel scalar through a time delay generator (DG645, SRS). The time-correlated single photon counting (TCSPC) is realized by the multichannel scalar with a time bin width of 5 ns.

First, the count rates of SPD2 under different pump levels are measured. Since the rate would be saturated if it were close to 100 kHz due to the dead time of SPD2 (10 μs), a modified count rate, denoted by C', is shown in Fig. 2. It is calculated by $C' = (C - d)/(1 - C \times \tau)$ [16], where C is the measured count rate of SPD2 and d and τ are the dark count rate and dead time of SPD2, respectively. Hence, C' is proportional to the real rate of photons arrived at SPD2, eliminating the impacts of counting saturation and dark counts. In Fig. 2, the up triangles are the measured results when both of the pumps are on and they have the same power denoted by P_{pump}. For comparison, results under single pump are also shown as the red dots and black squares, respectively. The down triangles are the sum of them. The photon counts under single pumps are due to

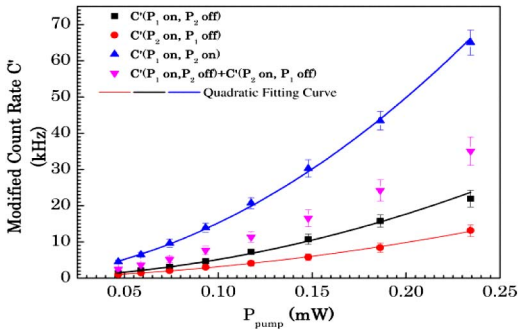

Fig. 2. Modified count rates (C') of SPD2 under different pumping condition and pump levels. The black square and red dots are the C' when only Pump1 or Pump2 is on. The down triangles are the sum of them, and the up triangles are the C' measured when both of the pumps are on. The lines are quadratic fitting curves of the experiment results.

the photons generated by the degenerate SFWM process. In this process, signal and idler photons are generated in different cavity modes; hence, they have no contribution to the photon pair generation in the specific cavity mode. It can be seen that C' measured when both pumps turn on is obviously higher than the sums of C' measured under a single pump. The increase in C' is due to the photon pairs generated by the nondegenerate SFWM. The lines in Fig. 2 are quadratic fitting curves of the experiment results, showing that the contributions of the degenerate SFWM and the nondegenerate SFWM all grow quadratically under increasing pump level.

To demonstrate the correlation of photon pairs generated by the nondegenerate SFWM, the coincidence and accidental coincidence counts of SPD1 and SPD2 are measured by the multichannel scalar, and then the ratios of coincidence to accidental coincidence (CAR) are calculated and shown in Fig. 3. Points in the figure are the statistical results of measurements. It can be seen that the measured CAR is far higher than 1, and rises with decreasing modified count rate of SPD2. The highest CAR is up to 100, which is realized under a C' of 4.5 kHz. It shows that, although the degenerate SFWM process leads to obvious noise photons, quantum correlation in the photon pairs generated by the nondegenerate SFWM process can be observed clearly.

Compared with previous works of high-performance photon pair generation in silicon microring cavities, the CAR is measured under relatively low pump levels in this experiment to avoid the impact of free carrier

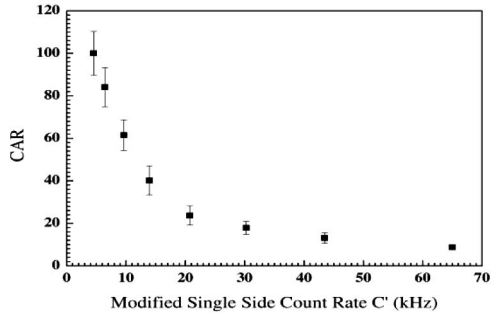

Fig. 3. CARs under different modified count rates of SPD2.

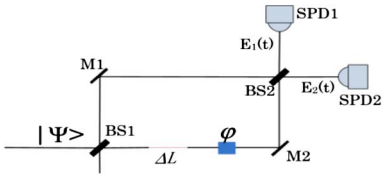

Fig. 4. Theoretical model for the quantum interference of the photon pairs in a MZI.

absorption in silicon waveguides and the dead time of the SPDs. It can be expected that high photon pair generation rate also can be realized under high pump levels in silicon microring cavities with reverse bias p-i-n structures, which is measured by superconducting nanowire SPDs [9]. It is also worth noting that, beside C', the CAR highly depends on the time bin width of TCSPC measurement [17]. A relatively wide time bin (5 ns) is used in this experiment. Higher CAR could be expected if smaller time bin width is applied (for comparison, a time bin width of ~230 ps is used in the experiment of Ref. [9]).

Then the quantum interference of the generated photon pairs in a Mach–Zehnder interferometer (MZI) is demonstrated. Figure 4 is the sketch for theoretical analysis, in which BS1 and BS2 are two beam splitters and M1 and M2 are two reflectors. The delay line provides a length difference between the two arms, which is denoted by ΔL. φ is a tunable phase difference between the two arms.

At the input port of the MZI, the photon pair state generated by the nondegenerate SFWM at the specific cavity mode can be expressed as [2,18]

$$|\psi\rangle = \int \mathrm{d}\omega_s \mathrm{d}\omega_i \Phi(\omega_s,\omega_i)\hat{a}_s^{\dagger}(\omega_s)\hat{a}_i^{\dagger}(\omega_i)|0\rangle$$
$$\Phi(\omega_s,\omega_i) = AF(\omega_s)F(\omega_i)\delta(\omega_{p1}+\omega_{p2}-\omega_s-\omega_i). \quad (1)$$

In this expression, ω_{p1} and ω_{p2} denote frequencies of the two pumps. ω_s and ω_i denote frequencies of generated signal and idler photons, respectively. A is a normalized coefficient. $F(\omega)$ is the enhancement factor of the cavity mode. If the cavity mode is under critical coupling (the cavity used in the experiment is close to critical coupling according to Table 1),

$$|F(\omega)|^2 = \frac{1}{|\kappa|^2[1+(\omega-\omega_0)^2/\delta\omega^2]}, \quad (2)$$

where ω_0 and δw are the resonance frequency and resonance line width of the cavity mode, respectively. κ is the coupling coefficient.

At output ports of the MZI before SPD1 and SPD2, the field operators can be expressed by [19]

$$\hat{E}_1(t) = -\frac{1}{2}\left[\hat{E}_s(t) - \hat{E}_s\left(t-\frac{\Delta L}{c}\right)e^{i\varphi} + \hat{E}_i(t) - \hat{E}_i\left(t-\frac{\Delta L}{c}\right)e^{i\varphi}\right],$$
$$\hat{E}_2(t) = \frac{i}{2}\left[\hat{E}_s(t) + \hat{E}_s\left(t-\frac{\Delta L}{c}\right)e^{i\varphi} + \hat{E}_i(t) + \hat{E}_i\left(t-\frac{\Delta L}{c}\right)e^{i\varphi}\right],$$

where

$$\hat{E}_{s,i}(t) = \frac{1}{\sqrt{2\pi}}\int \mathrm{d}\omega_{s,i}\hat{a}(\omega_{s,i})e^{-j\omega_{s,i}(t-z/c)}, \quad (3)$$

which are the field operators for signal and idler photons at the input end of the MZI.

The coincidence count rate of the SPD1 and SPD2 can be calculated by

$$R_{1,2} \propto \int_{T_R} G^{(2)}(\tau)\mathrm{d}\tau, \quad (4)$$

where T_R is the detection time for the measurement and $G^{(2)}(\tau)$ is the second-order correlation function, which can be calculated by

$$\begin{aligned} G^{(2)}(\tau) &= \langle \hat{E}_1^{\dagger}(t)\hat{E}_2^{\dagger}(t+\tau)\hat{E}_2(t+\tau)\hat{E}_1(t)\rangle \\ &= \frac{1}{16}\Big| g(0,\tau) + g(\tau,0) + g\left(0,\tau-\frac{\Delta L}{c}\right)e^{i\varphi} \\ &\quad + g\left(\tau-\frac{\Delta L}{c},0\right)e^{i\varphi} - g\left(-\frac{\Delta L}{c},\tau\right)e^{i\varphi} \\ &\quad - g\left(\tau,-\frac{\Delta L}{c}\right)e^{i\varphi} - g\left(-\frac{\Delta L}{c},\tau-\frac{\Delta L}{c}\right)e^{2i\varphi} \\ &\quad - g\left(\tau-\frac{\Delta L}{c},-\frac{\Delta L}{c}\right)e^{2i\varphi}\Big|^2. \end{aligned} \quad (5)$$

Here,

$$g(t_1,t_2) = \frac{1}{2\pi}\int \Phi(\omega_s,\omega_i)e^{-i\omega_s t_1 - i\omega_i t_2}\mathrm{d}\omega_s\mathrm{d}\omega_i. \quad (6)$$

Substituting Eqs. (1) and (2) into Eqs. (4)–(6), and given that T_R is long enough to extend the integration range of Eq. (4) to infinite, the coincidence count rate can be calculated as

$$R_{1,2} \propto \left(1 - \frac{1}{2}\left(1 + 2\delta\omega\cdot\frac{\Delta L}{c}\right)e^{-2\delta\omega\cdot\frac{\Delta L}{c}} - \frac{1}{2}\cos 2\varphi\right). \quad (7)$$

In the experiment, the MZI is realized by commercial DPSK demodulators. φ can be adjusted by the voltage applied to the DPSK demodulators and calibrated by another laser with narrow line width before each measurement. The experiment results under $\Delta L = 0$ and $\Delta L = 12$ cm are shown in Figs. 5(a) and 5(b), respectively. The black squares are measured coincidence counts (the contribution of accidental coincidence counts is subtracted), and the red lines are results of their sine fitting.

Equation (7) shows that, if $\Delta L = 0$, the coincidence count rate of SPD1 and SPD2 can be simplified to $R = 1 - \cos 2\varphi$. Hence, the two-photon interference fringe should have a sinusoidal dependence on φ with a period of π and a visibility of 100%. Figure 5(a) shows the experiment result under this case. It can be seen that the measured two-photon interference fringe has a period of π and a visibility of 95.4 ± 6.9%, agreeing well with the theoretical analysis, while the single side count of SPD2 has a sinusoidal dependence on φ with a period

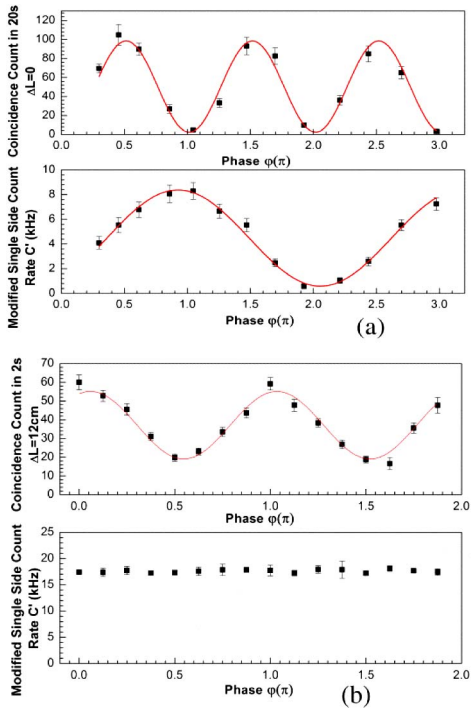

Fig. 5. Experiment results of the quantum interference of the generated degenerate-frequency photon pairs in a MZI. (a) $\Delta L = 0$ and (b) $\Delta L = 12$ cm.

of 2π, showing the interference of single-photon wave packets.

In the case of $\Delta L = 12$ cm, since line widths of two pumps are very narrow, the coherence length of the two-photon wave packet is far longer than ΔL, the interference of the two-photon state also can be expected. However, the coherence length of the single photon, which is determined by the resonance spectral width of the cavity mode, is smaller than the ΔL; hence, the interference of the single-photon wave packet is eliminated. The coincidence count rate can be calculated as $R \sim 1 - 1/2 \cos 2\pi$ according to Eq. (7), showing a theoretical visibility of 50%. Figure 5(b) shows experiment results in this case. The coincidence counts under different φ show a fringe with period π and visibility of $48.6 \pm 2.9\%$, close to 50%. While the single side count of SPD2 does not vary with φ, it also agrees with the theoretical analysis. These experiment results show that quantum interference can be realized by the generated degenerate-frequency photon pairs.

In conclusion, degenerate-frequency photon pairs at the telecom band are generated in a specific mode of a silicon microring cavity by the nondegenerate SFWM process under CW pumping. Maximum CAR is up to 100 under a time bin width of 5 ns, showing their characteristics of quantum correlation. The two-photon quantum interference in a MZI is demonstrated, showing a fringe visibility of $95.4 \pm 6.9\%$ in the balanced MZI and $48.6 \pm 2.9\%$ in the unbalanced MZI, which agrees with the theoretical analysis (100% for the balanced MZI and 50% for the unbalanced MZI), showing their potential in applications of quantum metrology and quantum information.

This work is supported in part by 973 Programs of China under Contract Nos. 2011CBA00303 and 2010CB327606, and NSFC Project under Contract No. 61321004.

References

1. J. E. Sharping, K. F. Lee, M. A. Foster, A. C. Turner, B. S. Schmidt, M. Lipson, A. L. Gaeta, and P. Kumar, Opt. Express **14**, 12388 (2006).
2. P. P. Absil, J. V. Hryniewicz, B. E. Little, P. S. Cho, R. A. Wilson, L. G. Joneckis, and P. T. Ho, Opt. Lett. **25**, 554 (2000).
3. H. Jung, C. Xiong, K. Y. Fong, X. F. Zhang, and H. X. Tang, Opt. Lett. **38**, 2810 (2013).
4. Z. Yang, P. Chak, A. D. Bristow, H. M. van Driel, R. Iyer, J. S. Aitchison, A. L. Smirl, and J. E. Sipe, Opt. Lett. **32**, 826 (2007).
5. S. Clemmen, K. P. Huy, W. Bogaerts, R. G. Baets, Ph. Emplit, and S. Massar, Opt. Express **17**, 16558 (2009).
6. S. Azzini, D. Grassani, M. J. Strain, M. Sorel, L. G. Helt, J. E. Sipe, M. Liscidini, M. Galli, and D. Bajoni, Opt. Express **20**, 23100 (2012).
7. S. Azzini, D. Grassani, M. Galli, L. C. Andreani, M. Sorel, M. J. Strain, L. G. Helt, J. E. Sipe, M. Liscidini, and D. Bajoni, Opt. Lett. **37**, 3807 (2012).
8. Q. Lin, O. J. Painter, and G. P. Agrawal, Opt. Express **15**, 16604 (2007).
9. E. Engin, D. Bonneau, C. M. Natarajan, A. S. Clark, M. G. Tanner, R. H. Hadfield, S. N. Dorenbos, V. Zwiller, K. Ohira, N. Suzuki, H. Yoshida, N. Iizuka, M. Ezaki, J. L. O'Brien, and M. G. Thompson, Opt. Express **21**, 27826 (2013).
10. M. Fiorentino, P. L. Voss, J. E. Sharping, and P. Kumar, IEEE Photon. Technol. Lett. **14**, 983 (2002).
11. J. Fan and A. Dogariu, Opt. Lett. **30**, 1530 (2005).
12. J. Chen, K. F. Lee, C. Liang, and P. Kumar, Opt. Lett. **31**, 2798 (2006).
13. J. P. Dowling, Contemp. Phys. **49**, 125 (2008).
14. E. Bimbard, N. Jain, A. MacRae, and A. I. Lvovsky, Nat. Photonics **4**, 243 (2010).
15. J. W. Silverstone, D. Bonneau, K. Ohira, N. Suzuki, H. Yoshida, N. Iizuka, M. Ezaki, C. M. Natarajan, M. G. Tanner, R. H. Hadfield, V. Zwiller, G. D. Marshall, J. G. Rarity, J. L. O'Brien, and M. G. Thompson, Nat. Photonics **8**, 104 (2013).
16. F. Zappa, A. Lacaita, S. Cova, and P. Lovati, Opt. Eng. **35**, 938 (1996).
17. S. Dong, Q. Zhou, W. Zhang, Y. He, W. Zhang, L. You, Y. Huang, and J. Peng, Opt. Express **22**, 359 (2014).
18. L. G. Helt, Z. Yang, M. Liscidiniand, and J. E. Sipe, Opt. Lett. **35**, 3006 (2010).
19. Z. Y. Ou, X. Y. Zou, L. J. Wang, and L. Mandel, Phys. Rev. Lett. **65**, 321 (1990).